FT-ICR Reaction Experiments and Molecular Dynamics Simulations of Precursor Clusters for SWNTs

Shigeo Maruyama

Department of Mechanical Engineering,
The University of Tokyo
7-3-1 Hongo, Bunkyo-ku, Tokyo 113-8656, Japan
TEL: 03-5841-6421 FAX: 03-5800-6983
E-Mail: maruyama@photon.t.u-tokyo.ac.jp

Abstract

The formation mechanism of single walled carbon nanotubes (SWNTs) is studied with cluster beam experiments and molecular dynamics simulations. A FT-ICR mass spectrometer directly connected to the laser-vaporization cluster beam source was employed to study the metal-carbon binary clusters generated by the laser-vaporization of Ni/Co loaded carbon materials used for the laser-furnace production of SWNTs. Enhanced production of C_{60}^+, C_{70}^+ and larger even-numbered pure carbon clusters in the size range up to 200 carbon atoms were observed for positive cluster ions. In clear contrast to the pure graphite, negative cluster ions up to about C_{200}^- with even numbers of carbon atoms were detected. In addition, small signals of NiC_n^-, CoC_n^- and $NiCoC_n^-$ were observed. The chemical reaction experiments of these clusters with NO strongly suggested that metal atoms were outside of the carbon cage. Eventually, some larger metal-carbon binary clusters with about 13 to 15 Co atoms were also observed. Complementally to cluster beam experiments, the growth process of metal-carbon clusters from completely random mixtures of vapor phase was simulated by the classical molecular dynamics method. A Ni atom on the face of the random cage prohibited the complete closure and anneal of the cage structure. Collisions of such imperfect random-cage clusters lead to the elongated caged structure, which can be regarded as an imperfect SWNT.

Introduction

After the discovery of C_{60} by Kroto *et al*. [1] in 1985, macroscopic amount of empty fullerene [2,3], endohedral metallofullerene [4-7], and higher fullerenes [8] were successively produced, isolated and characterized. The multi-walled carbon nanotubes (MWNTs) [9] and single walled carbon nanotubes (SWNTs)[10], which can be regarded as the especially elongated fullerene, were demonstrated by the fascinating TEM observations. Later, the high quality generation of SWNTs by the laser-furnace technique with Ni/Co-loaded graphite [11] and by the arc-discharge technique with Ni/Y-loaded graphite [12] were demonstrated. Here, generation conditions for SWNTs were almost identical to the empty fullerene and endohedral metallofullerene, except for the small amount of doped metal species. The catalytic chemical vapor deposition (CCVD) technique used efficiently for MWNTs production was modified for the generation of SWNTs [13-18]. Here, hydrocarbons such as CH_4 or C_2H_4 were decomposed with metals such as Fe, Ni, Co, Mo supported by Al_2O_3 or MgO fine

particles. Recently, metallocene $Fe(Co)_5$ [19] or metal-oxides solid solution [20] were used as the seed of metal nanoparticles without the support materials. Very recently, the almost amorphous free and scalable technique for the larger amount of SWNTs production was developed by using the gas-phase disproportionation reaction of high-pressure CO with $Fe(CO)_5$ as the catalyst seed [21].

Besides these innovations of new large-scale generation techniques, the formation mechanism of SWNTs has been intensively studied [22-36] through laser-furnace and arc-discharge experiments. Detailed studies with pulsed Nd: YAG laser [22-25, 27,29-34] experiments and CO_2 laser experiments [26] have revealed the dependence of SWNT diameter distribution on catalysts [25,30,31,33], temperature [29], pressure [22], laser pulse width [34] and flow rate [32]. Furthermore, measurements of laser plume emission and light scattering [26, 27, 32] gave the information of the growing materials. Similarly for arc-discharge method, effects of catalysts [28, 35] and temperature [36] were studied. Based on such experiments, several fascinating formation models of SWNTs have been proposed [11, 21, 23, 25]. Recently, a very interesting experiment was performed with the high-temperature pulse-arc discharge method [37]. The intermediate seed of SWNTs, which could be reheated to be SWNTs later, was generated without the sufficient furnace temperature. The similar two-stage generation process of SWNTs was made possible by the laser-furnace technique by decreasing the furnace temperature to about 800 °C during the laser ablation [38]. Hence, whole complicated process of generation of SWNTs can be separated into the initial 'precursor stage' and 'annealing/growth stage'.

In the initial stage of cluster formation in the laser-vaporization technique, the role of metal atoms is very striking. Empty fullerenes are generated with high yield without metal doping. With rare earth metals such as La, Y, and Sc, the endohedral metallofullerene is produced efficiently. Finally, with transition metals such as Ni/Co or Rh/Pd, seeds for high quality SWNTs are generated. The role of metal atoms for the completely different fates of carbon vapor is studied in this paper focusing on the initial 'precursor stage'.

We have already studied the metal-carbon binary clusters related to the endohedral metallofullerene by the laser-vaporization supersonic-expansion cluster beam source [39, 40]. Fourier Transform Ion Cyclotron Resonance (FT-ICR) mass spectrometer directly connected to the cluster source was implemented with the same basic design concept as at Rice University [41]. We have shown that positive La-C, Y-C, Sc-C, Gd-C, and Ce-C binary clusters commonly showed strong MC_{2n}^+ signal in the range of $36 < 2n < 76$ with intense magic numbers at MC_{44}^+, MC_{50}^+ and MC_{60}^+ [39] already at the cluster stage. Furthermore, in order to probe the structure of clusters appearing in mass spectra, the reactivity of negative carbon clusters and metal-carbon binary clusters to nitric oxide was measured and the existence of the metal atom inside the caged carbon clusters already at the cluster stage were demonstrated [40]. In this paper, by changing the metal species from those for endohedral metallofullerene to Ni/Co for SWNT generation, the metal-carbon binary clusters related to the SWNT generation were studied. Complimentary to the cluster beam studies, we have performed molecular dynamics simulations of the clustering process of carbon atoms to investigate the empty fullerene formation [42,43] and endohedral metallofullerene [44,45]. The formation of perfect C_{60} structure was demonstrated by giving sufficient annealing time after the cluster growth through random collisions. Based on these results, a formation model of empty fullerene through "random-cage" structure was proposed [43]. The

formation process of La- and Sc-encapsulated metallofullerene by the similar molecular dynamics simulations was compared with the cluster beam experiments [39, 40]. In this paper, a similar molecular dynamics simulation was performed with carbon and Ni system for the precursor clusters of SWNTs. By compressing the calculation cell to enhance the collision of those clusters, the possible structure as the result of successive collisions is explored.

FT-ICR Reaction Experiments

Fig. 1 shows the schematics of the FT-ICR mass spectrometer with direct-injection laser-vaporization cluster beam source. The design concept of this apparatus is the same as the FT-ICR apparatus in Smalley's group at Rice University [41]. In brief, the sample material was vaporized by the focused 2nd harmonics of Nd: YAG laser while a short pulse of He gas was injected. Intrinsic cluster ions produced at the laser-vaporization were directly injected to the superconducting 6 Tesla magnetic field. By adjusting the deceleration voltage and door voltages, roughly mass selected cluster ions were trapped in the ICR cell in the center of the magnetic field. Then, collisions with room temperature argon buffer gas at 10^{-5} Torr for typically 5 s followed for the thermalization. The as-injected cluster mass distribution was measured by exciting the cluster ions with the SWIFT technique [46].

Typical positive and negative 'as-injected' cluster ion distributions from Ni and Co (0.6 at % each) loaded graphite sample disk are shown in Fig.2. The positive cluster ion distribution is similar to the distribution obtained from a pure graphite sample [1,39]. Here, even numbered clusters of pure carbon atoms with dominant signals for C_{60} and C_{70} were observed, but no trace of Ni or Co was detected. However, careful comparison to the pure graphite case showed the considerable enhancement of C_{60} and C_{70}. We first thought that Ni or Co was helping the formation of more stable caged structure. However, there seems to be no reason that those metal atoms should enhance the production of pure C_{60} and C_{70}. Macroscopic experiments suggested considerable decrease of spherical fullerene at the optimum condition of SWNT generation. It seems more reasonable to assume that the relatively reactive "random cage" clusters were reacted away by the catalytic effect of metal atoms. Probably some clusters with metal atoms selectively attack those random cage clusters. Compared with the positive spectrum, negative mass spectrum is much busier. The negative mass spectrum in Fig. 2(b) is a little more extreme condition than typical negative spectra. Signals from Ni- and Co-attached carbon clusters are origin of this busy distribution as described in detail later. Furthermore, to some extent, the even-odd alternation of signal intensity is observed in the range from C_{30} through C_{60}. Another interesting feature is that the cluster ion distribution continued well beyond C_{60} range in clear contract to the negative ion distribution obtained from the pure graphite sample that usually rapidly decays at about the C_{60} mass range.

In order to confirm this point, the higher mass range was measured by adjusting the deceleration voltage as shown in Fig. 3. Here, both positive and negative mass spectra showed even-numbered carbon clusters in C_{120}-C_{160} range. Similar mass distributions were confirmed up to about the C_{300} range. Small signals between even-numbered negative cluster ions in Fig. 3(b) are odd-numbered carbon clusters. With the pure graphite sample, such even-numbered carbon clusters in such high mass range had never been detected for 'negative' cluster ions. These features may show that the metal

atoms or clusters strongly enhance the formation of large caged clusters. However, the strong negative even-numbered clusters may be due to the dissociation of positively charged metal atoms leaving an electron to the pure carbon clusters.

In order to distinguish Ni- or Co-attached clusters from pure carbon clusters, very detailed examination of isotope distributions is necessary, since Ni and Co have almost the same mass of 5 times of a carbon atom. Here, Co atom has a single natural isotope with 58.933 amu, but a Ni atom has 5 different natural isotopes (57.935amu: 68.077%, 59.931amu: 26.223%; 60.931amu: 1.14%; 61.928amu: 3.634%; 63.928amu: 0.926%). Since both metal atoms have about 0.07 amu shifts from integer atomic mass unit, this small shift of mass was used to count the number of metal atoms involved in the cluster signal. The comparison of simulated isotope distributions to the measure mass spectrum expanded in the mass range around 720 amu is shown in Fig. 4. For the complete fit to the experimental signal, considerable amount of $M_3C_{45}^-$ should also be included, but the fitting was so difficult with this limited resolution. It seems that a few atoms of Ni and Co attach to the carbon clusters almost evenly. In Fig. 2 (b), rather strong signals starting from 888 amu (or equivalent to mass of C_{74}) were observed. The preliminary fitting to the isotope distribution showed that these signals were due to $Co_{13}C_{10}$ and $Co_{13}C_{11}$. These were probably the large metal-carbon binary clusters similar to the well-known Met-Cars [47]. Since no post ionization of cluster beam was used in these experiments, some important large neutral clusters might be missing.

The chemical reaction experiments with NO were performed to obtain the information of those metal-carbon binary clusters. We have shown that NO is a convenient reactant gas to prove negative carbon clusters, since it was reactive enough and no charge transfer was observed [40]. The much less reactive feature of LaC_{2n}^- clusters compared with pure C_n^- clusters lead to the speculation that the La atom was inside the carbon cage at the cluster stage [40]. The 'as-injected' mass spectrum is shown in Fig. 5(a). Cluster ions trapped in the ICR cell were collided with room temperature Ar gas at 10^{-5} Torr for 10 s for the thermization. Then, without the selection of clusters, NO gas at 10^{-7} Torr was exposed for 2 s (Fig. 5(b)) or 10 s (Fig. 5(c)). The chemisorption of NO to NiC_{38} and CoC_{38} was observed at a much faster rate than the pure carbon clusters. It should be noticed that the pressure of NO was 1/100 times compared with the case of LaC_n experiments [40]. The reaction rate of CoC_n was a bit higher than NiC_n. After the reaction for 10 s, the product from pure carbon cluster C_nNO gradually appeared. Here, it can be concluded that the Ni- or Co-attached clusters were kept very reactive because of those metal atoms.

Molecular Dynamics Simulations

Theoretical contributions to the generation mechanism of carbon nanotubes are not straightforward since the system size and time scale are well beyond the simple simulation of whole process. Several previous classical molecular dynamics calculations have examined the specific points of generation mechanism such as open-end growth with and without nanometer scale metal particle [48], possibility of 'root-growth' precipitation [49], the lip-lip closure of MWNTs [50], open-end structure and stability of SWNTs [51], relation of elastic strain to experimental diameter distribution [52], and the stability depending on the tube diameter and length [53]. All these simulations employed Brenner potential [54] for the carbon only system since no reliable classical potential function between metal and carbon atoms is known.

We have constructed the classical potential function between carbon clusters and several metal atoms (La, Sc and Ni) for the molecular dynamics simulation of generation of endohedral metallofullerene [44, 45] based on DFT calculations of small metal-carbon binary clusters. The metal-carbon multi-body potential function was expressed as functions of carbon coordination number of a metal atom in a framework similar to the Brenner potential. The total potential energy was expressed as the sum of binding energy E_b as follows.

$$E_b = V_R + V_A + V_C \quad (1)$$

$$V_R = f(r_{ij}) \frac{D_e}{S-1} \exp\left\{-\beta\sqrt{2S}(r_{ij} - R_e)\right\} \quad (2)$$

$$V_A = -f(r_{ij}) \cdot B^* \frac{D_e S}{S-1} \exp\left\{-\beta\sqrt{2/S}(r_{ij} - R_e)\right\} \quad (3)$$

$$V_C = -f(r_{ij}) \frac{e^2}{4\pi\varepsilon_0} \frac{c_C c_M}{r_{ij}} \quad (4)$$

Here, r_{ij}, V_R and V_A denoted the distance between metal i and carbon j, Morse-type repulsive and attractive terms, respectively. The Coulomb term V_C was applied only to the La-C and Sc-C interactions with considerable charge transfer from the metal to carbon atoms. Potential parameters D_e, S, β, R_e, c_C, c_M listed in table 1 are related to potential depth, potential shape, potential width, equilibrium bond length, carbon charge, and metal charge, respectively.

The coordinate number of the metal atom N^C was defined using the cut-off function $f(r)$. Both the pre-factor to the attractive term B^*_{ij} and the electric charge c were expressed as functions of the coordinate number N^C. Considering the typical situation that a metal atom was surrounded by several carbon atoms, the effect of the bond angle between M-C bonds was ignored.

$$f(r) = \begin{cases} 1 & (r < R_1) \\ \left(1 + \cos\dfrac{r - R_1}{R_2 - R_1}\right)/2 & (R_1 < r < R_2) \\ 0 & (r > R_2) \end{cases} \quad (5)$$

$$N^C = 1 + \sum_{\text{carbon } k(\neq j)} f(r_{ik}) \quad (6)$$

$$B^* = \left\{1 + b(N^C - 1)\right\}^{\delta} \quad (7)$$

$$c_M = 3 - \exp(-k_1 N^C + k_2),\ c_C = c_M / N^C \quad (8)$$

Here, b and δ are potential parameters determining the decrease of energy according to the coordination number N^C. Potential parameters obtained by fitting to several DFT calculations of small metal-carbon clusters are listed in Table 1. Metal-metal interaction potentials were also constructed in the similar form [44, 45].

Using these potential functions in addition to the simplified [42] Brenner

potential for carbon-carbon interaction, the growth process of metal-carbon binary clusters was simulated. As the initial condition, the completely random vapor mixture of 2500 carbon and 25 Ni atoms were allocated in a 585 Å cubic fully periodic simulation cell. The high density of the system was compensated with the special temperature control method [42] at T_c = 3000 K. Fig. 6 shows a snapshot after 6 ns molecular dynamics calculation starting from the random gas phase initial condition. As shown in the inserted expanded views, many relatively large clusters up to about 100 carbon atoms and a few metal atoms were observed. Carbon clusters tended to be spherical random cage structure with a few metal atoms on the cage, which prevented from the complete closure of the cage structure. As in our previous simulations for empty fullerenes [43], the annealing simulations were necessary to obtain the final realistic structure. Annealing simulations for some of large clusters with a Ni atom at 2500 K resulted the quasi-periodic motion of the Ni atom flipping inside and outside of the carbon cage. The typical time scale of this flipping motion was about 5 to 10 ns depending on the carbon cage size. Due to this motion of the metal atom, there were almost always several dangling bonds in the carbon cage. On the other hand, empty even-numbered carbon clusters quickly annealed to the quasi-stable structure without dangling bonds. Then, they could eventually anneal to the more stable structure obeying the isolated pentagon rule (IPR) typically after about 100 ns. These cluster structures were qualitatively in good agreement with the FT-ICR experimental results. The qualitatively good agreement of the simulation results and the mass-spectroscopic results cannot exclude the possibility that small droplet of molten carbon with Ni and Co expels from the solid target [25], since the simulation assumes the complete gas phase initial condition and the FT-ICR experiment observes only the limited size range of clusters. However, at least some part of materials completely vaporized by the laser beam should follow the current structure of random-cage carbon cluster with attached metal atom.

Simply continuing the molecular dynamics simulation for the later stage may sound foolish by considering the real time scale of the generation process of SWNTs. Probably some nice connection to Monte Carlo approach [48] should be the best solution. However, in order to obtain the idea of the next collision stage, some more simulation was performed. Further simulation after the cluster formation in Fig. 6 was very time consuming since the collision rate was considerably slower. Even though it is expected that the collision rate may be even less at the later stage in real experimental condition, we slowly shrank the simulation cell to enhance the collisions. The shrinking rate was set as 6×10^{-5} Å per time step or about 12 m/s, which was much slower than the typical translational velocity of clusters. The final structure obtained after 4.5 ns shrinking simulation at 2000 K is shown in Fig. 7. Since most of random cage clusters observed in Fig. 6 were not completely closed they could easily coalesce at the relatively high temperature. This little too high temperature condition from the viewpoint of laser-oven experiment was chosen for a bit accelerated annealing within the limited simulation time scale. Even though the structure shown in Fig. 7 is rather too ugly, the tendency to be elongated network structure is clearly observed.

The annealing of a carbon network structure and migration of Ni atoms were relatively slow in this ‘time compressed’ simulation. However, the Ni atoms were slowly assembling to form clusters and were trying to find the most stable position, hemi-fullerene cap area. On the other hand, the elongated part tended to be made of pure carbon, and the network structure was annealing to SWNT structure. Given the

enough time for diffusion of metal atoms and network annealing, the structure may be a straight SWNT with metal clusters at each end. The further addition of random cage clusters may be preferentially occurs at these reactive end points.

Discussions

The catalytic effect of Ni atoms is not obvious in the simulation but the following explanation may be feasible for the entire process. At the clustering stage, Ni atoms simply attach to carbon clusters as shown in Fig. 6. Considering the atomic ratio of carbon to metals, such clusters with a few metal atoms with about 100 carbon atoms are very natural. FT-ICR mass spectra also support such structure to some extend. Here, it is expected that Ni atoms tend to stay on the carbon cage surface and prevent the complete closure and complete annealing to fullerene. Without these metal atoms stable fullerene will result, since normal fullerene generation techniques use exactly the same condition with laser-oven or arc-discharge apparatus except for the small amount of doped metals in the graphite rods. The major clusters observed in positive and negative mass-spectroscopy are simply even numbered carbon atoms, since the metal atoms are removed from such clusters through collisions with some more stable metal-carbon binary clusters similar to Met-Cars. Since the random cage carbon clusters are not stable as fullerene, they can easily make further growth by collisions each other. This collision leads to the elongated structure as shown in Fig. 7. The simulation time scale was way too short to reproduce the complete structure of single walled carbon nanotube, though.

References

1. H. W. Kroto, J. R. Heath, S. C. O'Brien, R. F. Curl, and R. E. Smalley, *Nature*, **318**, 162 (1985).
2. W. Krätschmer, L.D. Lamb, K. Fostiropoulos, and D. R. Huffman, *Nature*, **347**, 354 (1990).
3. R. E. Haufler, Y. Chai, L. P. F. Chibante, J. J. Conceicao, C. M. Jin, L. Wang, S. Maruyama, and R. E. Smalley, *Proc. Mat. Res. Soc. Symp.*, **206**, 627 (1991).
4. Y. Chai, T. Guo, C. M. Jin, R. E. Haufler, L. P. F. Chibante, J. Fure, L. Wang, J. M. Alford, and R. E. Smalley, *J. Phys. Chem.*, **95**, 7564 (1991).
5. H. Shinohara, H. Sato, Y. Saito, M. Ohkohchi and Y. Ando, *J. Phys. Chem.*, **96**, 3571 (1992).
6. Kikuchi, K., Suzuki, S., Nakano, Y., Nakahara, N., Wakabayashi, T., Shiromaru, H., Saito, K., Ikemoto, I. and Achiba, Y., *Chem. Phys. Lett.* **216**, 23 (1993).
7. Takata, M., Umeda, B., Nishibori, E., Sakata, M., Saito, Y., Ohno, M. and Shinohara, H., *Nature* **377**, 46 (1995).
8. K. Kikuchi, N. Nakahara, T. Wakabayashi, M. Honda, S. Suzuki, K. Saito, H. Shiromaru, K. Yamauchi, I. Ikemoto, T. Kuramochi, S. Hino, and Y. Achiba, *Chem. Phys. Lett.*, **188**, 177 (1992).
9. S. Iijima, *Nature*, **354**, 56 (1991).
10. S. Iijima and T. Ichihara, *Nature*, **363**, 603 (1993).
11. A. Thess, R. Lee, P. Nikolaev, H. Dai, P. Petit, J. Robert, C. Xu, Y. H. Lee, S. G. Kim, A. G. Rinzler, D. T. Colbert, G. E. Scuseria, D. Tomának, J. E. Fischer, and R. E. Smalley, *Science*, **273**, 483 (1996).

12. C. Journet, W. K. Maser, P. Bernier, A. Loiseau, M. L. de la Chapelle, S. Lefrant, P. Deniard, R. Lee, and J. E. Fisher, *Nature*, **388**, 756 (1997).
13. J. Kong, A. M. Cassell, and H. Dai, *Chem. Phys. Lett*., **292**, 567 (1998).
14. J. H. Hafner, M. J. Bronikowski, B. R. Azamian, P. Nikolaev, A. G. Rinzler, D. T. Colbert, K. A. Smith, and R. E. Smalley, *Chem. Phys. Lett*., **296**, 195 (1998).
15. H.M. Cheng, F. Li, X. Sun, S.D.M. Brown, M.A. Pimenta, A. Marucci, G. Dresselhaus, M.S. Dresselhaus, *Chem. Phys. Lett*. **289**, 602 (1998).
16. J.-F. Colomer, C. Stephan, S. Lefrant, G. V. Tendeloo, I. Willems, Z. Konya, A. Fonseca, Ch. Laurent, and J. B. Nagy, *Chem. Phys. Lett*., **317**, 83 (2000).
17. B. Liu, T. Wagberg, E. Olsson, R. Yang, H. Li, S. Zhang, H. Yang, G. Zou, B. Sundqvist, *Chem. Phys. Lett*. **320**, 365 (2000).
18. M. Su, B. Zheng and J. Liu, *Chem. Phys. Lett*., **322**, 321 (2000).
19. B. C. Satishkumar, A. Govindaraj, R. Sen, and C. N. R. Rao, *Chem. Phys. Lett*., **293**, 47 (1998).
20. E. Flahaut, A. Govindaraj, A. Peigney, Ch. Laurent, A. Rousset, C.N.R. Rao, *Chem. Phys. Lett*. **300**, 236 (1999).
21. P. Nikolaev, M. J. Bronikowski, R. K. Bradley, F. Rohmund, D. T. Colbert, K. A. Smith, and R. E. Smalley, *Chem. Phys. Lett*., **313**, 91 (1999).
22. M. Yudasaka, T. Komatsu, T. Ichihashi, Y. Achiba, and S. Iijima, *J. Phys. Chem. B*, **102**, 4892 (1998).
23. M. Yudasaka, T. Ichihashi, and S. Iijima, *J. Phys. Chem. B*, **102**, 10201 (1998).
24. M. Yudasaka, F. Kokai, K. Takahashi, R. Yamada, N. Sensui, T. Ichihashi, and S. Iijima, *J. Phys. Chem. B*, **103**, 3576 (1999).
25. M. Yudasaka, R. Yamada, N. Sensui, T. Wilkins, T. Ichihashi, and S. Iijima, *J. Phys. Chem. B*, **103**, 6224 (1999).
26. F. Kokai, K. Takahashi, D. Kasuya, T. Ichihashi, M. Yudasaka and S. Iijima, *Chem. Phys. Lett*. **332**, 449 (2000).
27. F. Kokai, K. Takahashi, M. Yudasaka, and S. Iijima, *J. Phys. Chem. B*, **104**, 6777 (2000).
28. M. Takizawa, S. Bandow, M. Yudasaka, Y. Ando, H. Shimoyama, and S. Iijima, *Chem. Phys. Lett*. **326**, 351 (2000).
29. S. Bandow, S. Asaka, Y. Saito, A.M. Rao, L. Grigorian, E., Richter, P.C. Eklund, *Phys. Rev. Lett*., **80**, 3779 (1998).
30. H. Kataura, A. Kimura, Y. Ohtsuka, S. Suzuki, Y. Maniwa, T. Hanyu, Y. Achiba, *Jpn. J. Appl. Phys*. **37**, L616 (1998).
31. H. Kataura, Y. Kumazawa, Y. Maniwa, I. Umezu, S. Suzuki, Y. Ohtsuka, Y. Achiba, *Synth. Metals* **103**, 2555 (1999).
32. R. Sen, Y. Ohtsuka, T. Ishigaki, D. Kasuya, S. Suzuki, H. Kataura, and Y. Achiba, *Chem. Phys. Lett*. **332**, 467 (2000).
33. O. Jost, A.A. Gorbunov, W. Pompe, T. Pichler, R. Friedlein, M. Knupfer, M. Reibold, H.-D. Bauer, L. Dunsch, M.S. Golden, J. Fink, *Appl. Phys. Lett*. **75**, 2217 (1999).
34. A.C. Dillon, P.A. Parilla, J.L. Alleman, J.D. Perkins, M.J. Heben, *Chem. Phys. Lett*., **316**, 13 (2000).
35. Y. Saito, Y. Tani, N. Miyagawa, K. Mitsushima, A. Kasuya, and Y. Nishina, *Chem. Phys. Lett*., **294**, 593 (1998).
36. M. Takizawa, S. Bandow, T. Torii, S. Iijima, Chem. Phys. Lett. 302, 146-150 (1999).

37. T. Sugai, H. Omote, S. Bandow, N. Tanaka, H. Shinohara, *J. Chem. Phys*., **112**, 6000 (2000).
38. Y. Achiba, private communication.
39. S. Maruyama, Y. Yamaguchi, and M. Kohno, T. Yoshida, *Fullerene Sci. Technol*., **7**-4, 621 (1999).
40. S. Maruyama, M. Kohno, and S. Inoue, *Fullerene 2000: Chemistry and Physics of Fullerenes and Carbon Nanomaterials*, ECS, 309 (2000)
41. S. Maruyama, L. R. Anderson and R. E. Smalley, *Rev. Sci. Instrum.*, **61**-12, 3686 (1990).
42. Y. Yamaguchi and S. Maruyama, *Chem. Phys. Lett.*, **286**, 336 (1998).
43. S. Maruyama and Y. Yamaguchi, *Chem. Phys. Lett.*, **286**, 343 (1998).
44. Y. Yamaguchi and S. Maruyama, *Euro. Phys. J. D*, **9,** 1-4, 385 (1999).
45. Y. Yamaguchi and S. Maruyama, *Fullerenes: Recent Advances in the Chemistry and Physics of Fullerenes and Related Materials*, vol. **7**, 640 (1999).
46. A. G. Marshall and F. R. Verdun, *Fourier Transforms in NMR, Optical, and Mass Spectrometry*, Elsevier, Amsterdam (1990).
47. S. F. Cartier, B. D. May, A. W. Castleman, *J. Phys. Chem*., **100**, 8175 (1996).
48. A. Maiti, C. J. Brabec, C. Roland, and J. Bernholc, *Phys. Rev. B*, **52**, 14850 (1995).
49. A. Maiti, C. J. Brabee, and J. Bernholc, *Phys. Rev. B*, **55**, R6097 (1997).
50. M. Buongiorno Nardelli, C. Brabec, A. Maiti, C. Roland, and J. Bernholc, *Phys. Rev. Lett*., **80**-2, 313(1998).
51. C.F. Cornwell, L.T. Wille, *Chem. Phys. Lett* **278**, 262 (1997).
52. C. F. Cornwell and L. T. Wille, *J. Chem. Phys*. **109**-2, 763 (1998).
53. S.B. Sinnott, R. Andrews, D. Qian, A.M. Rao, Z. Mao, E.C. Dickey, and F. Derbyshire, *Chem. Phys. Lett*., **315**, 25 (1999).
54. D. W. Brenner, *Phys. Rev. B*, **42**, 9458 (1990).

Table 1 Potential parameters for metal-carbon interactions.

	D_e (eV)	S	β (1/Å)	R_e (Å)	R_1 (Å)	R_2 (Å)	b	δ	k_1	k_2
La-C	4.53	1.3	1.5	2.08	3.2	3.5	0.0854	-0.8	0.0469	1.032
Sc-C	3.82	1.3	1.7	1.80	2.7	3.0	0.0936	-0.8	0.0300	1.020
Ni-C	3.02	1.3	1.8	1.70	2.7	3.0	0.0330	-0.8	-	-

Caption to Figures

Fig. 1. FT-ICR spectrometer with direct-injection laser-vaporization supersonic-expansion cluster beam source.

Fig. 2. Positive and negative mass spectra of clusters generated by the laser vaporization of Ni-Co loaded (0.6 at % each) graphite disk.

Fig. 3. Mass spectra of clusters generated from Ni/Co loaded sample in higher mass range.

Fig. 4. Expanded FT-ICR signal around 720 amu in Fig. 2 compared with the simulated isotropic distribution. The simulated distribution with metal atoms are marked as solid peaks. The relative abundance of C_{60}, $C_{60}H$, $C_{55}Co$, $C_{55}Ni$, and $C_{50}NiCo$ were assumed to be 100%, 50%, 40%, 40%, and 35%, respectively.

Fig. 5 Reaction of NiC_{38}^- and CoC_{38}^- with NO. Note that signal of pure carbon drawn in gray lines are out of scale.

Fig. 6 A snapshot of the clustering molecular dynamics simulation at 6 ns from initial random gas phase configuration. Large solid circles, empty circles, and gray circles represent Ni atoms, threehold-coordinated carbon atoms, other carbon atoms, respectively.

Fig. 7 The structure obtained after collisions of NiC_n clusters. All carbon atoms with threehold-coordination are not shown for clarity. Large solid circles and gray circles represent Ni atoms and carbon atoms with coordination other than threehold.

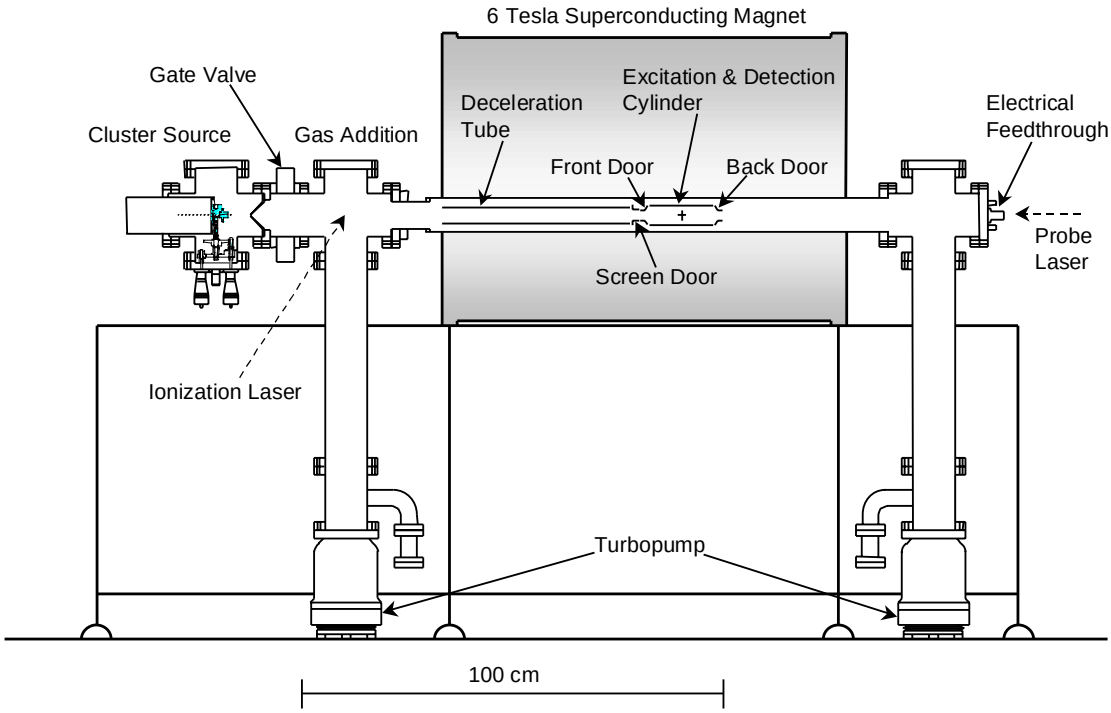

Fig. 1. FT-ICR spectrometer with direct-injection laser-vaporization supersonic-expansion cluster beam source.

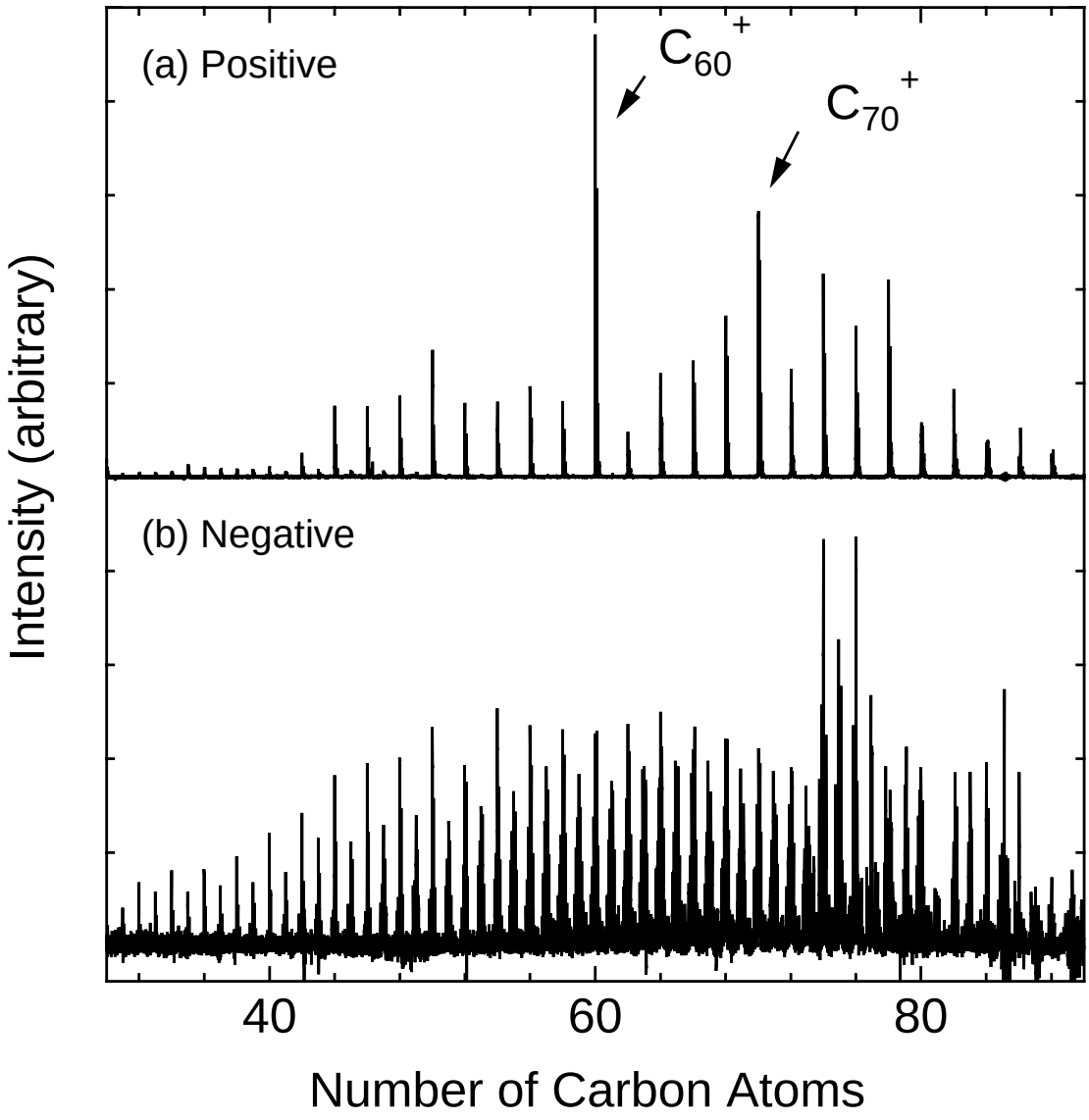

Fig. 2. Positive and negative mass spectra of clusters generated by the laser vaporization of Ni-Co loaded (0.6 at % each) graphite disk.

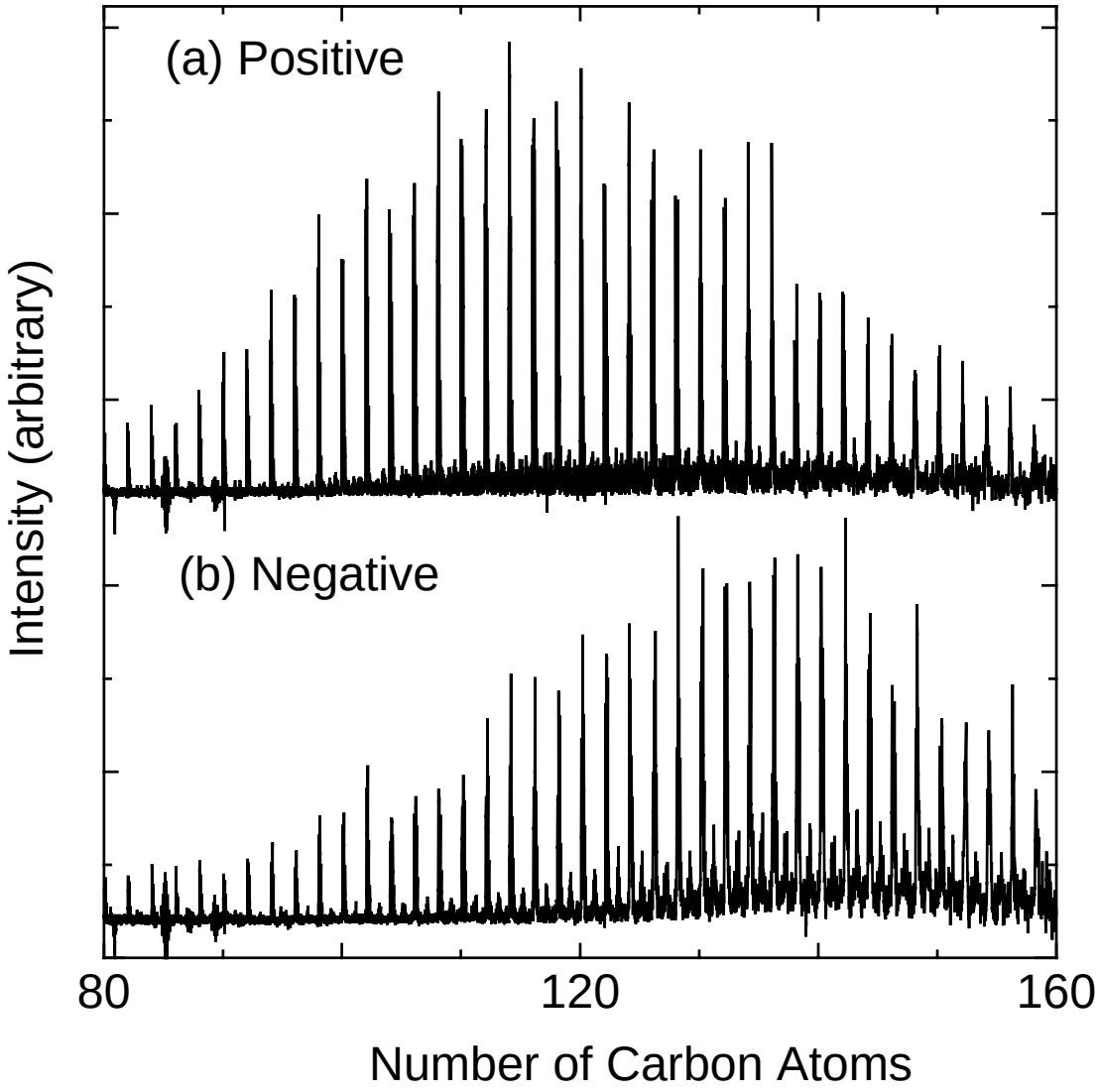

Fig. 3. Mass spectra of clusters generated from Ni/Co loaded sample in higher mass range.

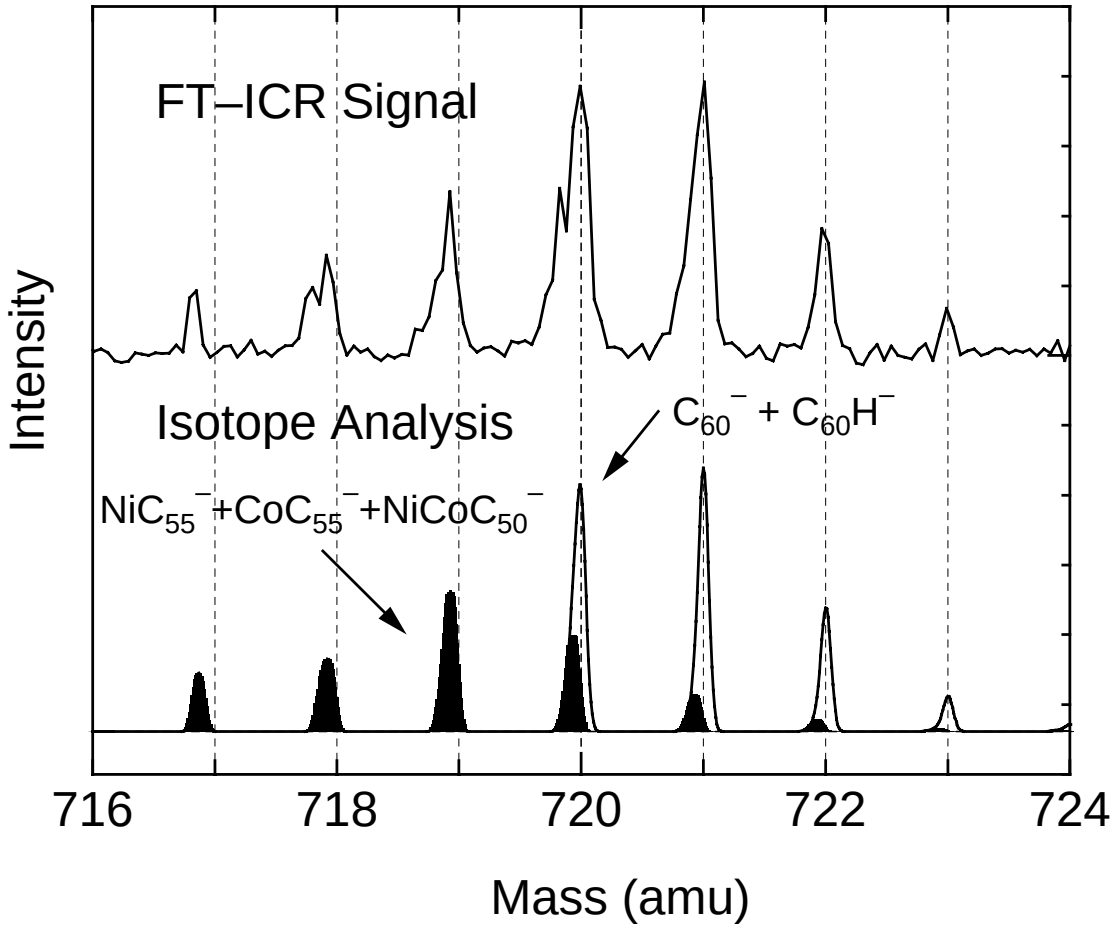

Fig. 4. Expanded FT-ICR signal around 720 amu in Fig. 2 compared with the simulated isotropic distribution. The simulated distribution with metal atoms are marked as solid peaks. The relative abundance of C_{60}, $C_{60}H$, $C_{55}Co$, $C_{55}Ni$, and $C_{50}NiCo$ were assumed to be 100%, 50%, 40%, 40%, and 35%, respectively.

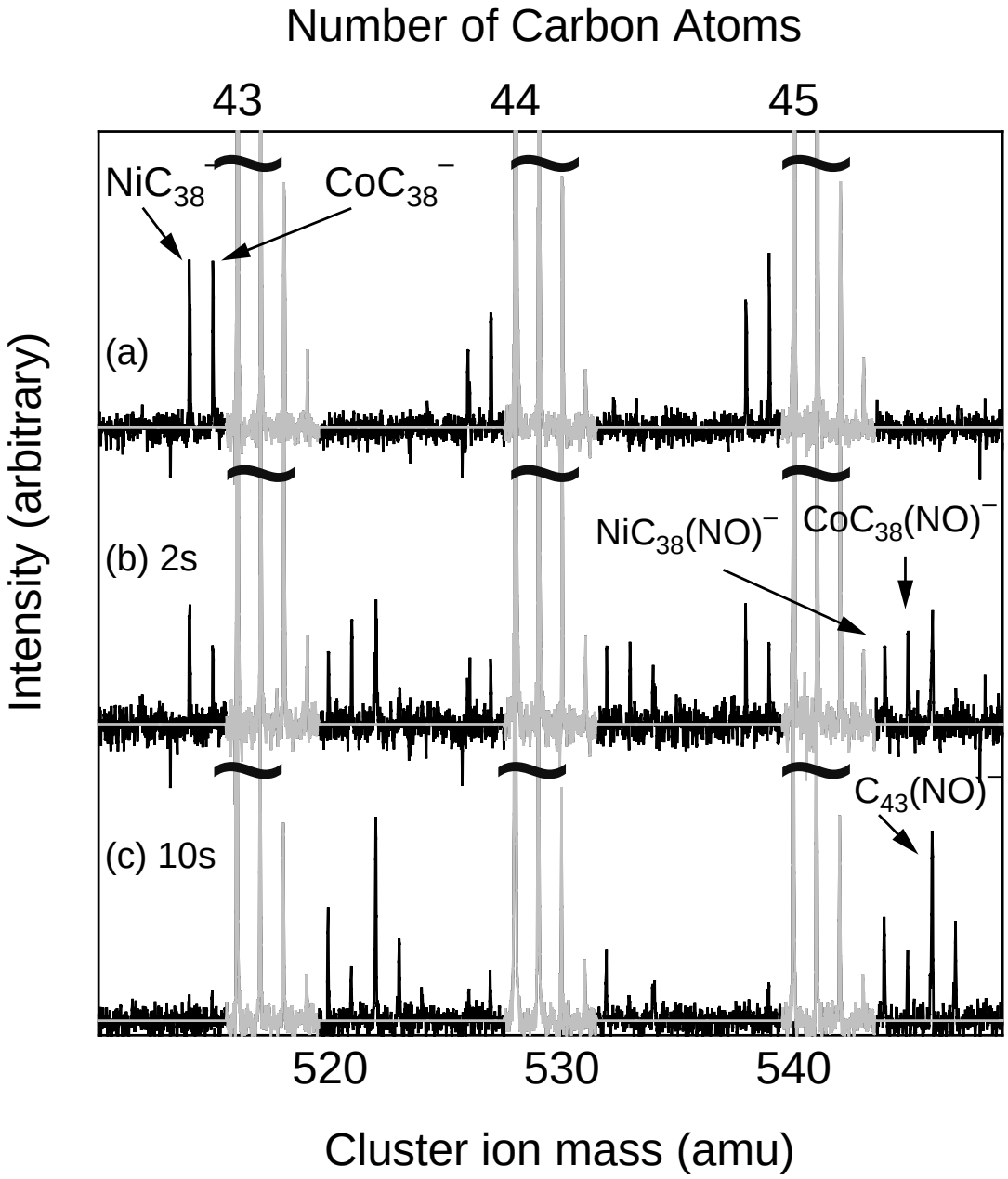

Fig. 5 Reaction of NiC_{38}^- and CoC_{38}^- with NO. Note that signal of pure carbon drawn in gray lines are out of scale.

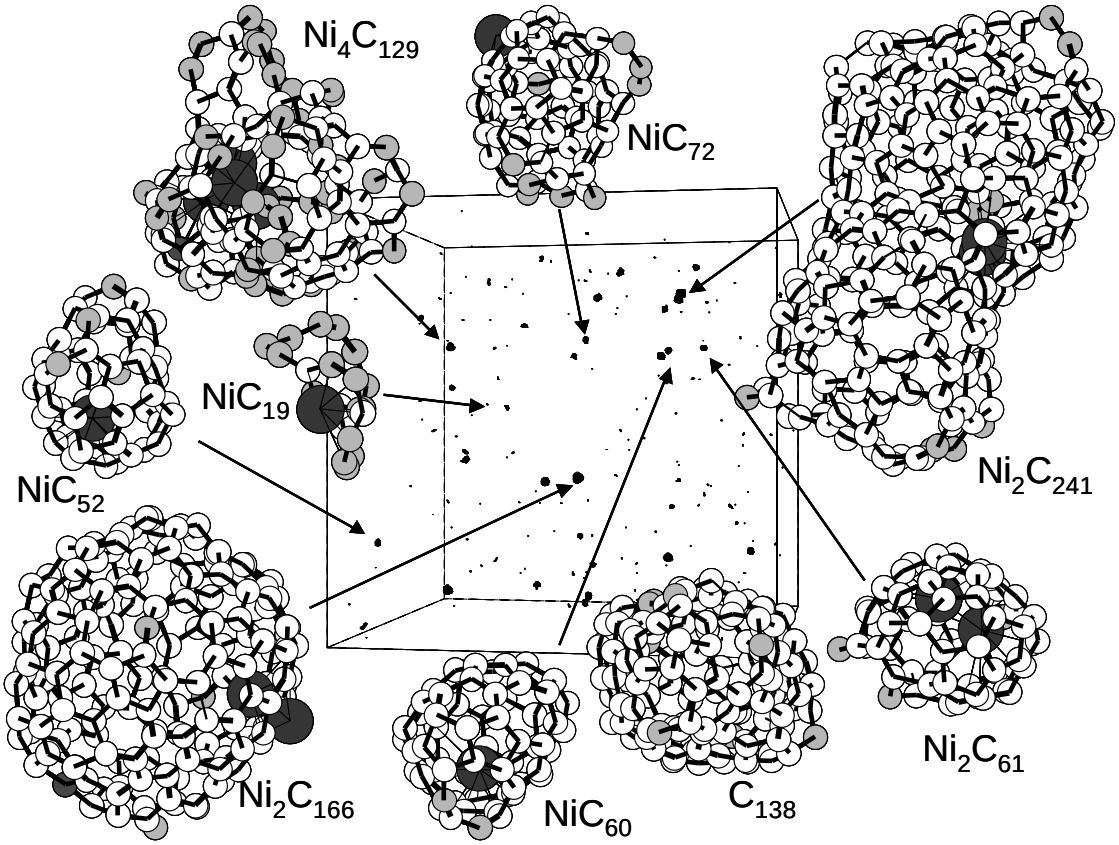

Fig. 6 A snapshot of the clustering molecular dynamics simulation at 6 ns from initial random gas phase configuration. Large solid circles, empty circles, and gray circles represent Ni atoms, threehold-coordinated carbon atoms, other carbon atoms, respectively.

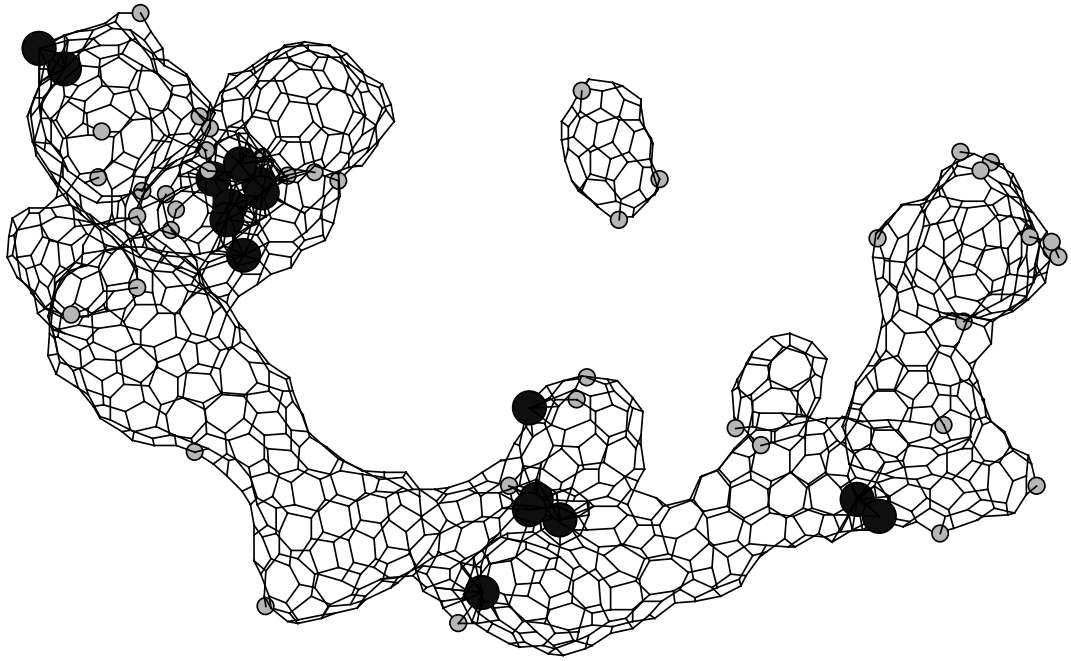

Fig. 7 Structure obtained after collisions of NiC_n clusters. All carbon atoms with threehold-coordination are not shown for clarity. Large solid circles and gray circles represent Ni atoms and carbon atoms with coordination other than threehold.